JACS
JOURNAL OF THE AMERICAN CHEMICAL SOCIETY
pubs.acs.org/JACS
Communication

3D Heteronuclear Magnetization Transfers for the Establishment of Secondary Structures in SARS-CoV-2-Derived RNAs

Jihyun Kim,[#] Mihajlo Novakovic,[#] Sundaresan Jayanthi, Adonis Lupulescu, Eriks Kupce, J. Tassilo Grün, Klara Mertinkus, Andreas Oxenfarth, Christian Richter, Robbin Schnieders, Julia Wirmer-Bartoschek, Harald Schwalbe, and Lucio Frydman*

Cite This: J. Am. Chem. Soc. 2021, 143, 4942−4948

ABSTRACT: Multidimensional NOESY experiments targeting correlations between exchangeable imino and amino protons provide valuable information about base pairing in nucleic acids. It has been recently shown that the sensitivity of homonuclear correlations involving RNA's labile imino protons can be significantly enhanced, by exploiting the repolarization brought about by solvent exchanges. Homonuclear correlations, however, are of limited spectral resolution, and usually incapable of tackling relatively large homopolymers with repeating structures like RNAs. This study presents a heteronuclear-resolved version of those NOESY experiments, in which magnetization transfers between the aqueous solvent and the nucleic acid protons are controlled by selecting specific chemical shift combinations of a coupled $^{1}H-^{15}N$ spin pair. This selective control effectively leads to a pseudo-3D version of HSQC-NOESY, but with cross-peaks enhanced by ∼2−5× as compared with conventional 2D NOESY counterparts. The enhanced signal sensitivity as well as access to both $^{15}N-^{1}H$ and $^{1}H-^{1}H$ NOESY dimensions can greatly facilitate RNA assignments and secondary structure determinations, as demonstrated here with the analysis of genome fragments derived from the SARS-CoV-2 virus.

RNAs fulfill numerous essential roles, including the propagation of genetic information, the regulation of expression, and support for protein synthesis.[1−4] Underlying this functional diversity is an equally diverse set of structures, of conformational dynamics, and of interactions with proteins, other nucleic acids, ligands, and ions, which NMR can explore with exquisite detail at physiological conditions.[5−12] Especially valuable in such analyses are the spectral signatures of the nitrogen-bound protons, which combine chemical shift resolution with valuable information about base pairing. NMR on RNAs thus usually starts with investigations of the imino and amino protons.[13−15] Imino resonances in particular appear at substantial downfield chemical shifts, well resolved from other ^{1}H peaks, and thereby facilitating RNA structural and binding studies.[7,16,17] Conspiring against a more widespread use of these resonances is their labile nature, as chemical exchanges with water broaden these peaks and complicate their observation.[18,19] Particularly hurt by chemical exchanges is the transfer of structurally relevant NOE information from the iminos/aminos to neighboring protons, a problem that further compounds the notoriously low signal-to-noise ratio (SNR) of NOESY cross-peaks.

Recently, we have proposed time-domain (L-PROSY[20]) and frequency-selective magnetization transfers (HMT[21]) methods that can bypass these complications, and substantially shorten imino- and amino-based RNA 2D NOESY experiments. As RNA constructs become larger, however, 2D homonuclear correlations become insufficient to distinguish all the protons involved. The chemically shifted attached nitrogens open the possibility to distinguish among these peaks—for instance, among guanosine and uracil imino resonances—making NOESY experiments involving heteronuclear editing/separation a valuable tool in RNA elucidations.[22] These experiments, however, are even more sensitivity-handicapped than their 2D homonuclear counterparts, since the additional heteronuclear transfer steps that they involve are also often compromised by the rapid imino↔water chemical exchanges.[23] Many resonances thus remain undetected in these experiments, or fail to generate NOESY cross peaks. The present study presents a way to alleviate this handicap based on what we denote as HETeronuclear MAgnetization Transfer (HETMAT) NOESY; a pseudo-3D NMR experiment making up for the aforementioned losses at the expense of readily available *a priori* information. HETMAT's substantial sensitivity enhancements of the ensuing $^{15}N-^{1}H-^{1}H$ correlations over conventional counterparts are shown here with structural elucidations from sizable fragments taken from the SARS-CoV-2 genome.

Figure 1a illustrates the idea proposed for recording these pseudo-3D $^{15}N-^{1}H$-resolved NOESY correlations. The experiment starts by assuming that the $^{15}N-^{1}H$ frequency pairs in the system are *a priori* known—for instance, from a preliminary heteronuclear 2D correlation—and that the positions of all such pairs are sufficiently resolved to be

Received: February 18, 2021
Published: March 30, 2021

https://doi.org/10.1021/jacs.1c01914
J. Am. Chem. Soc. 2021, 143, 4942−4948

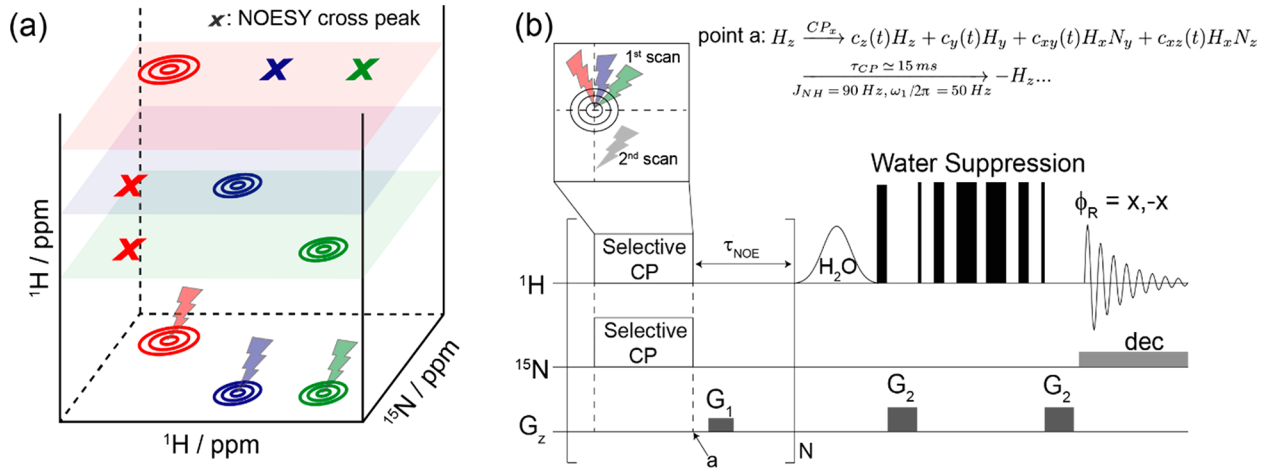

Figure 1. (a) Schematic representation of HETeronuclear MAgnetization Transfer (HETMAT), proposed for detecting HSQC-NOESY-type 3D correlations on labile sites. The experiment maps the NOE cross-peaks associated with a given ^{15}N−^{1}H spin pair along a third ^{1}H shift dimension, using 2D-frequency-specific saturations of the imino groups in the heteronuclear correlation plane. (b) Scheme proposed for executing HETMAT, based on looping selective cross-polarization (CP) modules that perturb the proton longitudinal magnetization for a specific ^{15}N−^{1}H frequency pair, leaving all other ^{1}Hs untouched. The selective longitudinal CP and an NOE mixing (τ_{NOE}) period are repeated n times to enhance the NOE cross-peaks by exchanges with the solvent, and the full spectrum is acquired with a scheme that suppresses the water signal. The selective CP is applied either on- or off-resonance in consecutive scans and data evaluated after receiver phase cycling ($\phi_R = x, -x$) in order to isolate the NOEs; "dec" indicates the ^{15}N decoupling used during the acquisition (see Supporting Information for additional details).

individually identified. Following the principles introduced in the HMT experiment,[21] the aim then is to selectively saturate or invert the ^{1}H peak associated with each such individual ^{15}N−^{1}H pair, so as to allow fast exchanges between these hydrogens and the solvent to reinstate the full magnitude of the NOE (or if inserting an isotropic mixing period, of the TOCSY) cross-peaks. Arraying such 1D experiment for every resolved heteronuclear ^{15}N−^{1}H spin pair then leads to a 3D information that is akin to that arising from an HSQC-NOESY (or HSQC-TOCSY)—but without suffering from the effects of fast exchanges with the solvent. With this as a guide, different approaches were assessed to selectively perturb a proton based on predefined ^{15}N−^{1}H frequency pairs. Selective versions of BIRD[24] and TANGO[25] were considered, yet the best performance for the desired 2D spectral manipulation was found in selective, longitudinal cross-polarization (CP) experiments.[26,27] Heteronuclear CP is normally used as a broadband technique in solids and liquids to transfer magnetizations between ^{1}H and X nuclei, as mediated by either J or dipolar couplings. However, narrowband versions of CP that selectively excite specific spin pairs according to their resonance offset have also been demonstrated.[28−30] In the present work, we relied on narrowband CP not to transfer polarization, but rather to selectively *invert* ^{1}H magnetizations for specific combinations of ^{1}H and ^{15}N offsets, i.e., as a first step in the HETMAT sequence. To perform this, simultaneous ^{1}H/^{15}N radiofrequency (RF) fields were applied on-resonance to an *a priori* selected imino group, while fulfilling the $\omega_{1H} = \omega_{1N} = \omega_1 \leq 2\pi J_{NH}$ Hartmann−Hahn matching condition.[31] Unlike a conventional CP, this does not spin-lock a transverse proton magnetization, but rather nutates it in a subspace composed from single (H) and two-spin (HN) operators.[32] Assuming that the RF fields are applied along the x-axes of the spins' doubly rotating frames, it can be shown (see Supporting Information) that the evolution starting from an initial H_z polarization is then

$$H_z \xrightarrow{CP_x} c_Z(t)H_z + c_Y(t)H_y + c_{XY}(t)H_xN_y + c_{XZ}(t)H_xN_z \tag{1}$$

where the $\{c\}_{i=Z,\,Y,\,XY,\,XZ}$ describe the time-dependent coefficients for each spin operator. To maximize the subsequent Overhauser cross-relaxation of a proton thus excited, we seek to achieve an inversion—or at least the largest possible perturbation away from equilibrium—of the initial H_z. Restricting for concreteness the discussion to on-resonance Hartmann−Hahn matching conditions, the relevant dynamics are then

$$c_Z^{on}(t) = \cos\left(\frac{\pi J_{NH} t}{2}\right)\cos\left(\sqrt{4\omega_1^2 + \pi^2 J_{NH}^2}\,\frac{t}{2}\right) + \sin\left(\frac{\pi J_{NH} t}{2}\right)\sin\left(\sqrt{4\omega_1^2 + \pi^2 J_{NH}^2}\,\frac{t}{2}\right)\left(\frac{\pi J_{NH}}{\sqrt{4\omega_1^2 + \pi^2 J_{NH}^2}}\right) \tag{2}$$

(Other coefficients and comparisons are given in the Supporting Information (SI)). To evaluate the Overhauser effects arising from such an inversion, a second, reference scan is also acquired, where Hartmann−Hahn matching conditions are no longer fulfilled. To do so, the ^{15}N offset is shifted far off-resonance (Figure 1b); H_Z's time-dependence then becomes

$$c_Z^{off}(t) = \frac{\pi^2 J_{NH}^2 + \omega_1^2 \cos(\sqrt{\omega_1^2 + \pi^2 J_{NH}^2}\,t)}{\omega_1^2 + \pi^2 J_{NH}^2} \tag{3}$$

With these expressions for $c_Z^{on}(t)$ and $c_Z^{off}(t)$ coefficients for a given J_{NH}, it is possible to find optimal ω_1 and mixing time τ_{CP} values that maximize their absolute difference—and hence the magnitude of the subsequent homonuclear NOE. For certain cases like $\omega_1/2\pi = 2J_{NH}$, this can be done analytically: $\tau_{CP} = 1/\pi J_{NH}$ will then lead to optimal $c_Z^{on} = -1$, $c_Z^{off} = +1$ conditions. Spectral selectivity, however, generally demands working with

https://doi.org/10.1021/jacs.1c01914
J. Am. Chem. Soc. 2021, 143, 4942−4948

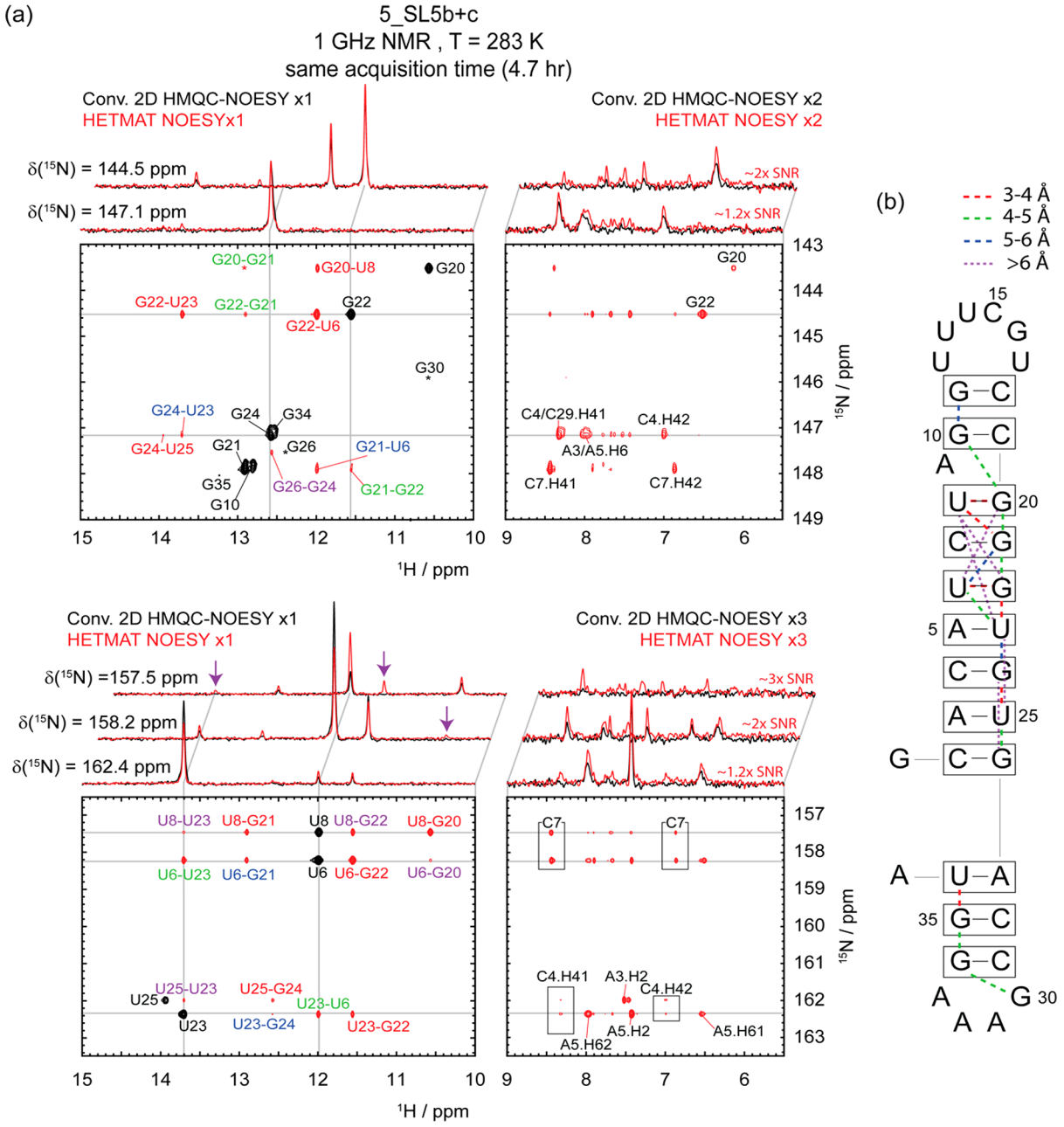

Figure 2. (a) HETMAT and 2D HMQC NOESY data showing imino−imino and imino−amino proton correlations for the SARS-CoV-2-derived 5_SL5b+c RNA fragment in (b), measured at 1 GHz and 283 K. To facilitate viewing of the 3D HETMAT data, contours were projected into the ^{15}N−^{1}H plane, with black and red contours used to represent the NOESY diagonal and cross-peaks, respectively. Assignments reported for these diagonal and cross-peaks are annotated in red, green, blue, and purple according to the predicted distances; among the peaks labeled in purple, G26-G24, U8-U23, U8-G22, and U6-G20 are cross-peak correlations observed in the HETMAT NOESY but not in the HMQC-NOESY experiment. Shown on top for comparison are 1D slices extracted at the indicated ^{15}N shifts from conventional 2D HMQC-NOESY (175 ms mixing, black) and HETMAT NOESY (red), collected on the same sample using identical acquisition times. For the HETMAT NOESY acquisitions, RF fields $\omega_1/2\pi$ = 75 Hz with 20 loops and a τ_{NOE} = 30 ms for mixing were used for the faster exchanging G35 residue; for all the rest, a CP with $\omega_1/2\pi$ = 50 Hz and 7 loops with τ_{NOE} = 125 ms mixing were used. (b) Secondary structure of 5_SL5b+c; dashed lines denote the correlations observed by HETMAT between specific base pairs, color-coded according to their estimated distances. See SI Figure S11 for a 3D rendering of the indicated connectivities.

$\omega_1/2\pi \leq J_{NH}$. Given prototypical J_{NH} = 90 Hz values, we chose working with $\omega_1/2\pi$ = 50 Hz; for these conditions, eqs 2 and 3 predict a τ_{CP} = 16 ms for maximizing $|c_Z^{on} - c_Z^{off}|$. This is in good agreement with the τ_{CP} = 15 ms measured experimentally on RNAs for achieving maximal HETMAT NOEs (SI Figure S2). SI Figures S3 and S4 further analyze the inversion efficiency and the chemical shift selectivity achieved under these conditions, showing that sizable $|c_Z^{on} - c_Z^{off}| > 1$ perturbations can be achieved, and that spectral resolutions of ca. ± 50 and ±25 Hz then characterize the ^{1}H and ^{15}N dimensions, respectively. This selectivity sufficed for targeting our SARS-CoV-2-derived RNA fragments when studied at 1 GHz (23.5 T), but led to some peak cross-talk when examined at 600 MHz (SI Figure S4). The sensitivity with which this selective

https://doi.org/10.1021/jacs.1c01914
J. Am. Chem. Soc. 2021, 143, 4942−4948

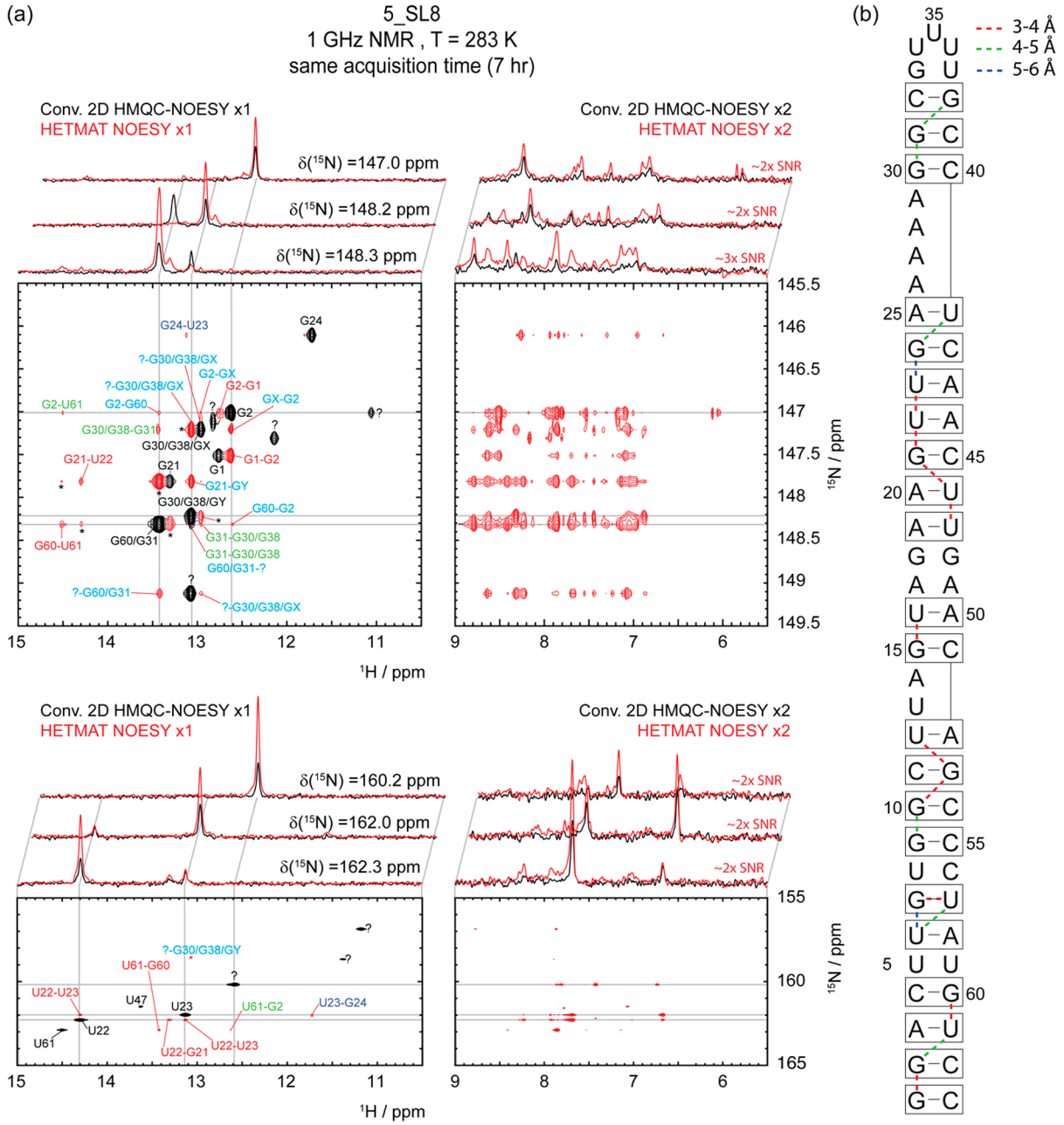

Figure 3. (a,b) Idem as in Figure 2, but for the larger 5_SL8 fragment shown on the right. The color-code used here is akin to that in Figure 2, except that diagonal peaks with uncertain assignments are labeled with black question ("?") marks, and ambiguous off-diagonal counterparts are marked by question marks, or by GX, GY labels. Newly observed NOE correlations are labeled in cyan. Asterisks indicate artificial signals arising due to insufficient selectivity; 1D slices from conventional HMQC-NOESY (150 ms mixing) and HETMAT NOESY are shown on top. For the broader peaks, an RF CP field $\omega_1/2\pi$ = 75 Hz with 17 loops and τ_{NOE} = 50 ms mixing was used; otherwise, CP with $\omega_1/2\pi$ = 50 Hz and 10 loops with τ_{NOE} = 80 ms mixing were used. Notice that at this field HETMAT NOESY has sufficient selectivity to resolve peaks with very similar ^{15}N chemical shifts (e.g., $\delta(^{15}N)$ = 148.2 and 148.3 ppm, traces on top); this ability decreased at lower fields (SI Figure S7). The apparent difference in resolution between the guanosine and uridine peaks (top and bottom contours) reflects the different chemical shift ranges plotted along F_1 in each case. See SI Figure S11 for a 3D rendering of this structure, showing the indicated connectivities.

CP subtraction provided its ^{1}H−^{15}N correlations was comparable to or larger than that arising from conventional HSQC or HMQC experiments (SI Figure S4a); while higher CP fields ω_1 could increase the sensitivity further, this would be achieved at the expense of sacrificing spectral resolution. These efficient, selective heteronuclear inversions were then looped as previously described,[17,18] for the sake of enhancing the iminos' NOE correlations.

The method described above was employed in the analysis of two SARS-CoV-2-derived RNA fragments, seeking to introduce heteronuclear resolution in imino−imino and imino−amino ^{1}H−^{1}H NOE correlations. As peak assignments for the smallest of the targeted fragments, the 5_SL5b+c domain of SARS-CoV-2's RNA, have been reported,[33] experiments were collected on this fragment mainly for sensitivity comparisons. All the diagonal and cross-peaks in the fragment's ^{15}N−^{1}H HSQC and ^{1}H−^{1}H NOESY spectra

https://doi.org/10.1021/jacs.1c01914
J. Am. Chem. Soc. 2021, 143, 4942−4948

are clearly identified by HETMAT spectra acquired at 1 GHz (Figure 2). Besides the additional spectral dimension available in HETMAT NOESY thanks to the heteronuclear separation, significant SNR enhancements are evidenced when this experiment is compared against conventional 2D counterparts of the same duration (Figure 2, on top of each panel; notice that since conventional 3D HSQC-NOESY acquisitions on this sub-mM sample would take days to complete, 2D HMQC-NOESY versions of the experiment were used in this comparison). Note as well that several imino−imino correlations—including those between U8-G22, U8-U23, U6-G20, and G24-G26 (purple arrows and fonts in the spectra)—are only detected by HETMAT NOESY. As some of these distances exceed 5 Å, the possibility that they reflect spin-diffusion effects cannot be discarded. Additional examples of HETMAT's sensitivity advantage over its HMQC-based counterpart for this sample are presented in SI Figure S5.

The performance of the HETMAT NOESY experiment is further illustrated in Figure 3, for the larger SARS-CoV-2-derived 5_SL8 RNA fragment. In this case, 2D HMQC-NOESY cannot resolve all the proximate peaks even at 1 GHz—for instance, the traces arising from $\delta(^{15}N)$ = 148.2 and 148.3 ppm—leading to the multiple identical NOE cross-peak patterns due to overlapping signal contributions. By introducing a heteronuclear dimension, HETMAT can help identify the individual NOE correlations for each imino proton, while enjoying a substantial gain in sensitivity. Furthermore, as illustrated and exploited by the results in Figures 2 and 3, HETMET's focusing on one specific residue per scan enables tailoring both the heteronuclear CP fields as well as the details of the NOE mixing, to the chemical and spectral nature of the residue being tackled. Better-resolved residues can thus be studied with higher RFs leading to shorter CPs, while correlations to broad sites characterized by enhanced solvent exchanges can be studied using more loops and shorter τ_{NOE}s. Additional comparisons between HETMAT and HMQC-based experiments for this sample are shown in SI Figures S6 and S7. The latter highlights results obtained at a lower field, where resolution becomes more limited for closely positioned peaks.

Despite the selectivity provided by the combination of narrowband CP and the use of high magnetic fields, 5_SL8 is a case where total site resolution is not feasible even at 1 GHz. SI Figure S8 exemplifies this for a region where the selective CP for a residue denoted as peak 1, simultaneously labeling a second residue peak 2. This notwithstanding, and as a result of the cross-talk's asymmetric behavior between the peaks, unambiguous NOE correlations end up becoming achievable by comparing the HETMAT spectra for peaks 1 and 2. This is typical for complex RNA structures such as this one, where differential solvent exchange rates of the individual iminos involved in the cross-relaxation can end up breaking the symmetry of otherwise identical RF manipulations. Peaks marked by asterisks in Figure 3 illustrate other instances where the narrowband CP was insufficiently selective to separate closely spaced $^{15}N-^{1}H$ peaks, yet where similar analyses as in Figure S8 allowed us to identify genuine NOE correlations originating from these groups. In this respect, it is worth noting that the rates of solvent exchange and the relaxation properties of the protons may limit HETMAT's potential gains: the experiment's sensitivity will usually be larger when magnetization is transferred from fast-exchanging to slow-exchanging protons. This can explain why certain cross-correlations fail to show up, even if involving base pairs in adjacent positions. While this makes certain peak assignments still ambiguous, HETMAT's improved resolution and sensitivity gains allowed us to establish a number of imino proton correlations that had not been previously reported.[33]

In summary, a novel experiment that can enhance the sensitivity and resolution of homonuclear NOESY correlations by targeting selected $^{1}H-^{15}N$ spin pairs was introduced for targeting labile protons. The resolution of the resulting experiment—particularly at high fields—ended up comparable to that of 3D acquisitions. This was achieved by using selective longitudinal CP for incorporating the heteronuclear information: by avoiding reliance on coherent polarization transfers to/from the heteronucleus, this route also helped increase the overall sensitivity. Selective CP requires *a priori* knowledge of the 2D $^{15}N-^{1}H$ correlations; in return, it enables customizing the saturation/inversion conditions, mixing time and number of loops *N*, to each individual residue. As solvent exchanges vary widely among NHs, and as they can be assessed *a priori* by the broadness of the targeted ^{1}H peak, this customization helps maximize the NOE enhancements. This selectivity also helped enhance the effective resolution among overlapping sites, using asymmetric buildup considerations. HETMAT's sensitivity gains can also enable studies at higher, physiologically relevant temperatures, despite the increase in chemical exchange rates. This is illustrated in SI Figure S9, which shows that although both HETMAT- and HMQC-based NOESYs suffer upon increasing temperatures as a result of faster exchanges, HETMAT can still deliver a very similar information content as obtained at lower temperatures. This opens interesting possibilities to investigate RNA structures at physiological conditions. Another intriguing possibility exists upon working under mismatched Hartman-Hahn conditions (Figure S10), which according to simulations and experiments could increase the NOE-derived cross-peaks about 50% compared to matched CP conditions, while allowing lower ω_1 fields and thus better spectral selectivity. It also remains to be seen to what extent these gains associated with frequency-domain manipulations can be preserved, as spectral crowding in the heteronuclear plane increases.

■ ASSOCIATED CONTENT

Supporting Information

The Supporting Information is available free of charge at https://pubs.acs.org/doi/10.1021/jacs.1c01914.

Experimental section; Time evolution of an I_z state upon establishing longitudinal cross-polarization on- and off-the Hartmann−Hahn conditions; HETMAT's inversion efficiency, $^{15}N-^{1}H$ spectral selectivity and sensitivity vs HMQC-NOESY on SARS-CoV-2 fragments; Improving HETMAT's spectral selectivity; HETMAT vs HMQC-NOESY performances at room temperature; HETMAT's improved sensitivity under off-Hartmann−Hahn conditions; HETMAT NOESY connectivities in the putative 3D structures of the 5_SL5b+c and 5_SL8 SARS-CoV-2 fragments; additional HETMAT vs HMQC-NOESY comparisons recorded at 600 MHz (PDF)

https://doi.org/10.1021/jacs.1c01914
J. Am. Chem. Soc. 2021, 143, 4942−4948

AUTHOR INFORMATION

Corresponding Author

Lucio Frydman − *Department of Chemical and Biological Physics, Weizmann Institute of Science, Rehovot 7610001, Israel;* orcid.org/0000-0001-8208-3521; Email: lucio.frydman@ weizmann.ac.il

Authors

Jihyun Kim − *Department of Chemical and Biological Physics, Weizmann Institute of Science, Rehovot 7610001, Israel*

Mihajlo Novakovic − *Department of Chemical and Biological Physics, Weizmann Institute of Science, Rehovot 7610001, Israel*

Sundaresan Jayanthi − *Department of Physics, Indian Institute of Space Science and Technology, Thiruvananthapuram 695 547, Kerala, India;* orcid.org/0000-0003-3957-1022

Adonis Lupulescu − *Aleea Nicolae Titulescu nr. 8, Turda, 407405 Judeţul Cluj, Romania*

Eriks Kupce − *Bruker Ltd, Coventry CV4 9GH, United Kingdom;* orcid.org/0000-0002-2366-0269

J. Tassilo Grün − *Institute of Organic Chemistry and Chemical Biology, Center for Biomolecular Magnetic Resonance, Johann Wolfgang Goethe-University, D-60438 Frankfurt/Main, Germany*

Klara Mertinkus − *Institute of Organic Chemistry and Chemical Biology, Center for Biomolecular Magnetic Resonance, Johann Wolfgang Goethe-University, D-60438 Frankfurt/Main, Germany*

Andreas Oxenfarth − *Institute of Organic Chemistry and Chemical Biology, Center for Biomolecular Magnetic Resonance, Johann Wolfgang Goethe-University, D-60438 Frankfurt/Main, Germany*

Christian Richter − *Institute of Organic Chemistry and Chemical Biology, Center for Biomolecular Magnetic Resonance, Johann Wolfgang Goethe-University, D-60438 Frankfurt/Main, Germany*

Robbin Schnieders − *Institute of Organic Chemistry and Chemical Biology, Center for Biomolecular Magnetic Resonance, Johann Wolfgang Goethe-University, D-60438 Frankfurt/Main, Germany*

Julia Wirmer-Bartoschek − *Institute of Organic Chemistry and Chemical Biology, Center for Biomolecular Magnetic Resonance, Johann Wolfgang Goethe-University, D-60438 Frankfurt/Main, Germany*

Harald Schwalbe − *Institute of Organic Chemistry and Chemical Biology, Center for Biomolecular Magnetic Resonance, Johann Wolfgang Goethe-University, D-60438 Frankfurt/Main, Germany;* orcid.org/0000-0001-5693-7909

Complete contact information is available at: https://pubs.acs.org/10.1021/jacs.1c01914

Author Contributions

[#]J.K. and M.N. contributed equally.

Funding

This work was supported by the EU Horizon 2020 program (FET-OPEN Grant 828946, PATHOS), Israel Science Foundation Grants 965/18 and 3572/20, Weizmann's "Kill Corona" Fund, and the Perlman Family Foundation. H.S. was supported by the Goethe Corona Funds, EU-supported iNEXT-discovery, and by DFG-funded collaborative research center 902. Work at BMRZ is supported by the state of Hesse. Joint support to LF, HS was given by the German-Israel Foundation (grant G-1501−302).

Notes

The authors declare the following competing financial interest(s): Eriks Kupce is an employee of Bruker Ltd.

ACKNOWLEDGMENTS

We are grateful to Dr. Tali Scherf for help with the 1 GHz measurements. L.F. holds the Bertha and Isadore Gudelsky Professorial Chair and Heads the Clore Institute for High-Field Magnetic Resonance Imaging and Spectroscopy, whose support is acknowledged.

ABBREVIATIONS

HETMAT NOESY, HETeronuclear MAgnetization Transfer Nuclear Overhauser Efffect SpectroscopY; CP, cross-polarization; SNR, signal-to-noise ratio.

REFERENCES

(1) Ambros, V. The Functions of Animal MicroRNAs. *Nature* **2004**, *431* (7006), 350−355.

(2) Hannon, G. J.; Rossi, J. J. Unlocking the Potential of the Human Genome with RNA Interference. *Nature* **2004**, *431* (7006), 371−378.

(3) He, L.; Hannon, G. J. MicroRNAs: Small RNAs with a Big Role in Gene Regulation. *Nat. Rev. Genet.* **2004**, *5* (7), 522−531.

(4) Mattick, J. S. RNA Regulation: A New Genetics? *Nat. Rev. Genet.* **2004**, *5* (4), 316−323.

(5) Varani, G.; Aboul-ela, F.; Allain, F. H.-T. NMR Investigation of RNA Structure. *Prog. Nucl. Magn. Reson. Spectrosc.* **1996**, *29* (1), 51−127.

(6) Wu, M.; Tinoco, I. RNA Folding Causes Secondary Structure Rearrangement. *Proc. Natl. Acad. Sci. U. S. A.* **1998**, *95* (20), 11555−11560.

(7) Fürtig, B.; Richter, C.; Wöhnert, J.; Schwalbe, H. NMR Spectroscopy of RNA. *ChemBioChem* **2003**, *4* (10), 936−962.

(8) Buck, J.; Fürtig, B.; Noeske, J.; Wöhnert, J.; Schwalbe, H. Time-Resolved NMR Methods Resolving Ligand-Induced RNA Folding at Atomic Resolution. *Proc. Natl. Acad. Sci. U. S. A.* **2007**, *104* (40), 15699−15704.

(9) Rinnenthal, J.; Buck, J.; Ferner, J.; Wacker, A.; Fürtig, B.; Schwalbe, H. Mapping the Landscape of RNA Dynamics with NMR Spectroscopy. *Acc. Chem. Res.* **2011**, *44* (12), 1292−1301.

(10) Lombès, T.; Moumné, R.; Larue, V.; Prost, E.; Catala, M.; Lecourt, T.; Dardel, F.; Micouin, L.; Tisné, C. Investigation of RNA−Ligand Interactions by 19F NMR Spectroscopy Using Fluorinated Probes. *Angew. Chem.* **2012**, *124* (38), 9668−9672.

(11) Calabrese, D. R.; Connelly, C. M.; Schneekloth, J. S.; Hargrove, A. E. Chapter Seven - Ligand-Observed NMR Techniques to Probe RNA-Small Molecule Interactions. *Methods in Enzymology* **2019**, *623*, 131−149.

(12) Becette, O. B.; Zong, G.; Chen, B.; Taiwo, K. M.; Case, D. A.; Dayie, T. K. Solution NMR Readily Reveals Distinct Structural Folds and Interactions in Doubly 13C- and 19F-Labeled RNAs. *Sci. Adv.* **2020**, *6* (41), eabc6572.

(13) Neuhaus, D.; Williamson, M. P. The Nuclear Overhauser Effect in Stereochemical and Conformational Analysis. In *Methods in Stereochemical Analysis*; John Wiley: New York, 2000.

(14) Cavanagh, J.; Skelton, N. J.; Fairbrother, W. J.; Rance, M. *Protein NMR Spectroscopy: Principles and Practice*; Elsevier, 2010.

(15) Wüthrich, K. *NMR of Proteins and Nucleic Acids*; Wiley, 1986.

(16) Latham, M. P.; Zimmermann, G. R.; Pardi, A. NMR Chemical Exchange as a Probe for Ligand-Binding Kinetics in a Theophylline-Binding RNA Aptamer. *J. Am. Chem. Soc.* **2009**, *131* (14), 5052−5053.

(17) Lee, M.-K.; Gal, M.; Frydman, L.; Varani, G. Real-Time Multidimensional NMR Follows RNA Folding with Second Resolution. *Proc. Natl. Acad. Sci. U. S. A.* **2010**, *107* (20), 9192−9197.
(18) Schnieders, R.; Wolter, A. C.; Richter, C.; Wöhnert, J.; Schwalbe, H.; Fürtig, B. Novel 13C-Detected NMR Experiments for the Precise Detection of RNA Structure. *Angew. Chem., Int. Ed.* **2019**, *58* (27), 9140−9144.
(19) Schnieders, R.; Keyhani, S.; Schwalbe, H.; Fürtig, B. More than Proton Detection—New Avenues for NMR Spectroscopy of RNA. *Chem. - Eur. J.* **2020**, *26* (1), 102−113.
(20) Novakovic, M.; Cousin, S. F.; Jaroszewicz, M. J.; Rosenzweig, R.; Frydman, L. Looped-PROjected SpectroscopY (L-PROSY): A Simple Approach to Enhance Backbone/Sidechain Cross-Peaks in 1H NMR. *J. Magn. Reson.* **2018**, *294*, 169−180.
(21) Novakovic, M.; Kupče, E.; Oxenfarth, A.; Battistel, M. D.; Freedberg, D. I.; Schwalbe, H.; Frydman, L. Sensitivity Enhancement of Homonuclear Multidimensional NMR Correlations for Labile Sites in Proteins, Polysaccharides, and Nucleic Acids. *Nat. Commun.* **2020**, *11* (1), 5317.
(22) Peterson, R. D.; Theimer, C. A.; Wu, H.; Feigon, J. New Applications of 2D Filtered/Edited NOESY for Assignment and Structure Elucidation of RNA and RNA-Protein Complexes. *J. Biomol. NMR* **2004**, *28* (1), 59−67.
(23) Mueller, L.; Legault, P.; Pardi, A. Improved RNA Structure Determination by Detection of NOE Contacts to Exchange-Broadened Amino Protons. *J. Am. Chem. Soc.* **1995**, *117* (45), 11043−11048.
(24) Garbow, J. R.; Weitekamp, D. P.; Pines, A. Bilinear Rotation Decoupling of Homonuclear Scalar Interactions. *Chem. Phys. Lett.* **1982**, *93* (5), 504−509.
(25) Wimperis, S.; Freeman, R. An Excitation Sequence Which Discriminates between Direct and Long-Range CH Coupling. *J. Magn. Reson. 1969* **1984**, *58* (2), 348−353.
(26) Pines, A.; Shattuck, T. W. Carbon-13 Proton NMR Cross-polarization Times in Solid Adamantane. *J. Chem. Phys.* **1974**, *61* (3), 1255−1256.
(27) Garroway, A. N.; Chingas, G. C. Creation of J-Ordered Magnetic States by Adiabatic Demagnetization in the Rotating Frame. *J. Magn. Reson. 1969* **1980**, *38* (1), 179−184.
(28) Pelupessy, P.; Chiarparin, E. Hartmann−Hahn Polarization Transfer in Liquids: An Ideal Tool for Selective Experiments. *Concepts Magn. Reson.* **2000**, *12* (3), 103−124.
(29) Korzhnev, D. M.; Orekhov, V. Yu.; Kay, L. E. Off-Resonance R1ρ NMR Studies of Exchange Dynamics in Proteins with Low Spin-Lock Fields: An Application to a Fyn SH3 Domain. *J. Am. Chem. Soc.* **2005**, *127* (2), 713−721.
(30) Kobzar, K.; Luy, B. Spin state selective Hadamard encoding during transfer periods using multiple selective CW-HCP. *J. Magn. Reson.* **2007**, *186*, 228−237.
(31) Hartmann, S. R.; Hahn, E. L. Nuclear Double Resonance in the Rotating Frame. *Phys. Rev.* **1962**, *128* (5), 2042−2053.
(32) Parella, T. A Complete Set of Novel 2D Correlation NMR Experiments Based on Heteronuclear J-Cross Polarization. *J. Biomol. NMR* **2004**, *29* (1), 37−55.
(33) Wacker, A.; Weigand, J. E.; Akabayov, S. R.; Altincekic, N.; Bains, J. K.; Banijamali, E.; Binas, O.; Castillo-Martinez, J.; Cetiner, E.; Ceylan, B.; Chiu, L.-Y.; Davila-Calderon, J.; Dhamotharan, K.; Duchardt-Ferner, E.; Ferner, J.; Frydman, L.; Fürtig, B.; Gallego, J.; Grün, J. T.; Hacker, C.; Haddad, C.; Hähnke, M.; Hengesbach, M.; Hiller, F.; Hohmann, K. F.; Hymon, D.; de Jesus, V.; Jonker, H.; Keller, H.; Knezic, B.; Landgraf, T.; Löhr, F.; Luo, L.; Mertinkus, K. R.; Muhs, C.; Novakovic, M.; Oxenfarth, A.; Palomino-Schätzlein, M.; Petzold, K.; Peter, S. A.; Pyper, D. J.; Qureshi, N. S.; Riad, M.; Richter, C.; Saxena, K.; Schamber, T.; Scherf, T.; Schlagnitweit, J.; Schlundt, A.; Schnieders, R.; Schwalbe, H.; Simba-Lahuasi, A.; Sreeramulu, S.; Stirnal, E.; Sudakov, A.; Tants, J.-N.; Tolbert, B. S.; Vögele, J.; Weiß, L.; Wirmer-Bartoschek, J.; Wirtz Martin, M. A.; Wöhnert, J.; Zetzsche, H. Secondary Structure Determination of Conserved SARS-CoV-2 RNA Elements by NMR Spectroscopy. *Nucleic Acids Res.* **2020**, *48* (22), 12415−12435.

https://doi.org/10.1021/jacs.1c01914
J. Am. Chem. Soc. 2021, 143, 4942−4948